Supplementary Information (SI) for

Disorder and residual helicity alter p53-Mdm2 binding affinity and signaling in cells

Wade Borcherds, François-Xavier Theillet, Andrea Katzer, Ana Finzel, Katie M. Mishall, Anne T. Powell, Hongwei Wu, Wanda Manieri, Christoph Dieterich, Philipp Selenko, Alexander Loewer and Gary W. Daughdrill

Supplementary Results
Supplementary Figure 1

Borcherds *et al.*

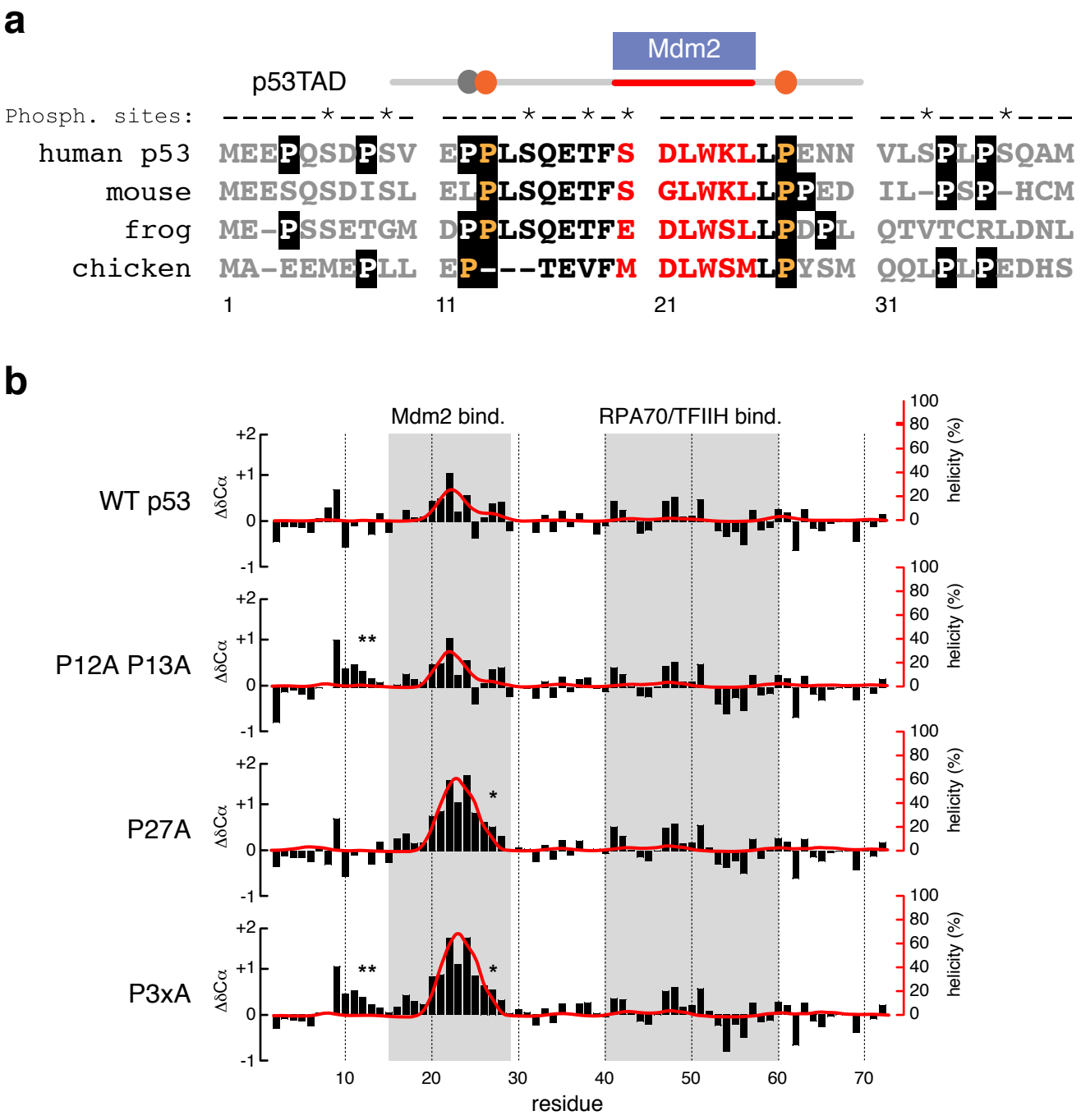

Supplementary Figure Legends

Supplementary Figure 1: Conservation of proline residues and degrees of transient helicity of WT and mutant p53TAD

a) Multiple sequence alignment of vertebrate p53TADs. Conserved prolines flanking the Mdm2 binding site (red) are shown in orange. **b)** Extended random-coil α carbon chemical shift deviations (ΔδCα, black bars) and helical d2D plots (red) for WT and mutant p53TADs as determined by NMR spectroscopy. Asterisks denote sites of proline to alanine mutations. Grey shadings depict p53 residues involved in Mdm2 and RPA70/TFIIH binding.

Supplementary Figure 2 Borcherds *et al.*

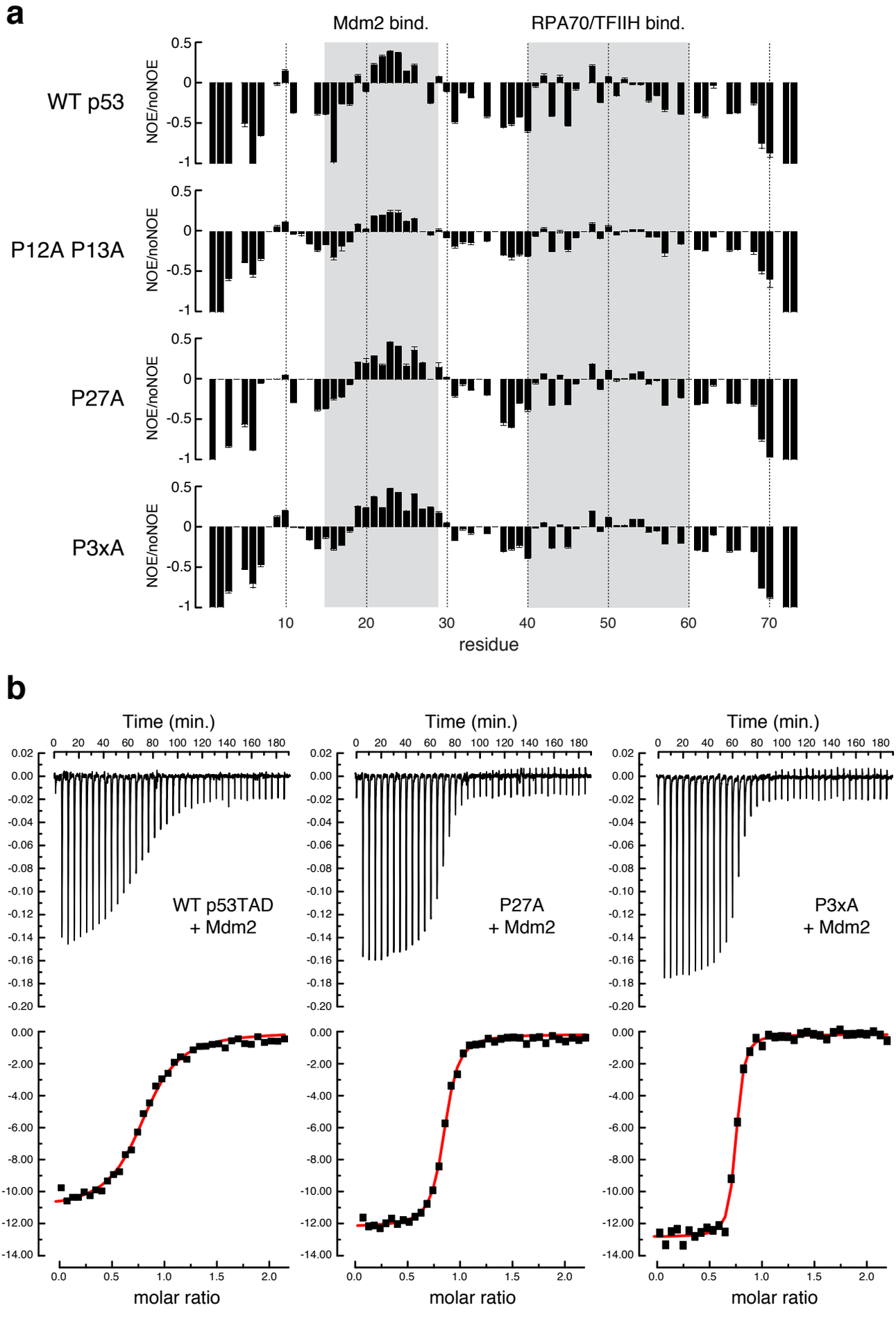

Supplementary Figure 2: Backbone dynamics of p53TAD and affinity measurements for Mdm2 binding

a) Hetero-nuclear NHNOE data for free WT and mutant p53TAD (aa1-73). Values are the average of three replicate experiments. Error bars denote standard deviations. **b)** Exemplary ITC traces of WT and mutant p53TAD binding to Mdm2.

a

	% helicity	Kd (nM)	ΔG (kcal/mol)	ΔH (kcal/mol)	-TΔS (kcal/mol)
WT p53	**28**	240 ± 60	-9.1 ± 0.2	-11.6 ± 0.4	2.4 ± 0.4
P12A P13A	**32**	220 ± 30	-9.1 ± 0.1	-11.6 ± 0.4	2.5 ± 0.4
P27A	**64**	25 ± 3	-10.4 ± 0.1	-12.1 ± 0.1	1.7 ± 0.1
P3xA	**66**	17 ± 6	-10.6 ± 0.2	-14.0 ± 0.3	3.3 ± 0.5

b

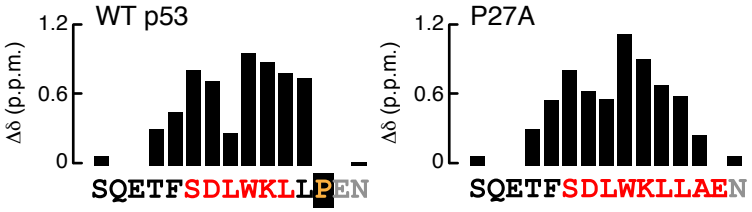

c

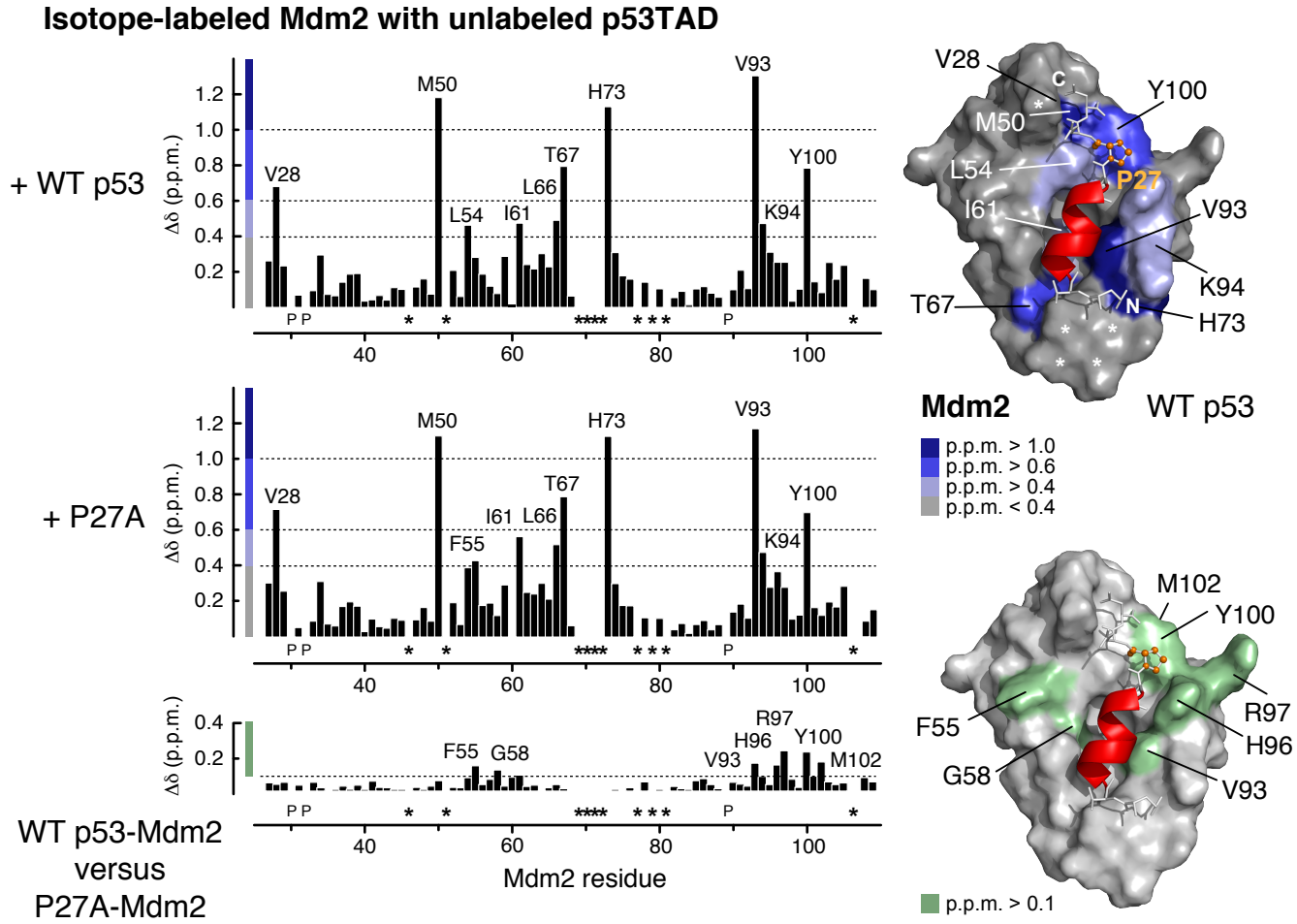

Supplementary Figure 3: Binding characteristics of WT and mutant p53TAD to Mdm2

a) Extended panel of thermodynamic binding parameters of WT and mutant p53TAD-Mdm2 interactions. **b)** Combined ^{1}H, ^{15}N chemical shift differences ($\Delta\delta = [\Delta\delta(^{1}H)^{2} + (\Delta\delta(^{15}N)/5)^{2}]^{1/2}$) of ^{15}N isotope-labeled WT and mutant p53TAD (aa1-73) upon binding to unlabeled Mdm2. No p53TAD backbone amide chemical shifts greater than 0.25 p.p.m were detected outside the shown interaction region. **c)** Combined ^{1}H, ^{15}N chemical shift differences ($\Delta\delta$) of ^{15}N isotope-labeled Mdm2 (aa17-125) upon binding to unlabeled WT and P27A p53TAD. Residues experiencing chemical shift changes greater than 0.4 p.p.m are labeled and color-coded in shades of blue. Surface mapping identifies highly congruent binding effects of WT and P27A p53TAD on Mdm2 (pdb code: 1YCR). Mdm2 prolines are indicated. Asterisks denote sites of intermediate chemical exchange, line-broadening and absence of chemical shift information in the respective complexes. Note that despite the lack of data for these sites, their positions are conserved in both complexes. *Bottom panel:* Chemical shift difference ($\Delta\delta$) mapping between WT and P27A p53TAD-Mdm2 complexes confirms similar binding modes and highlights minor local effects experienced by Mdm2 residues 93-103 at the p53 proline to alanine mutation site.

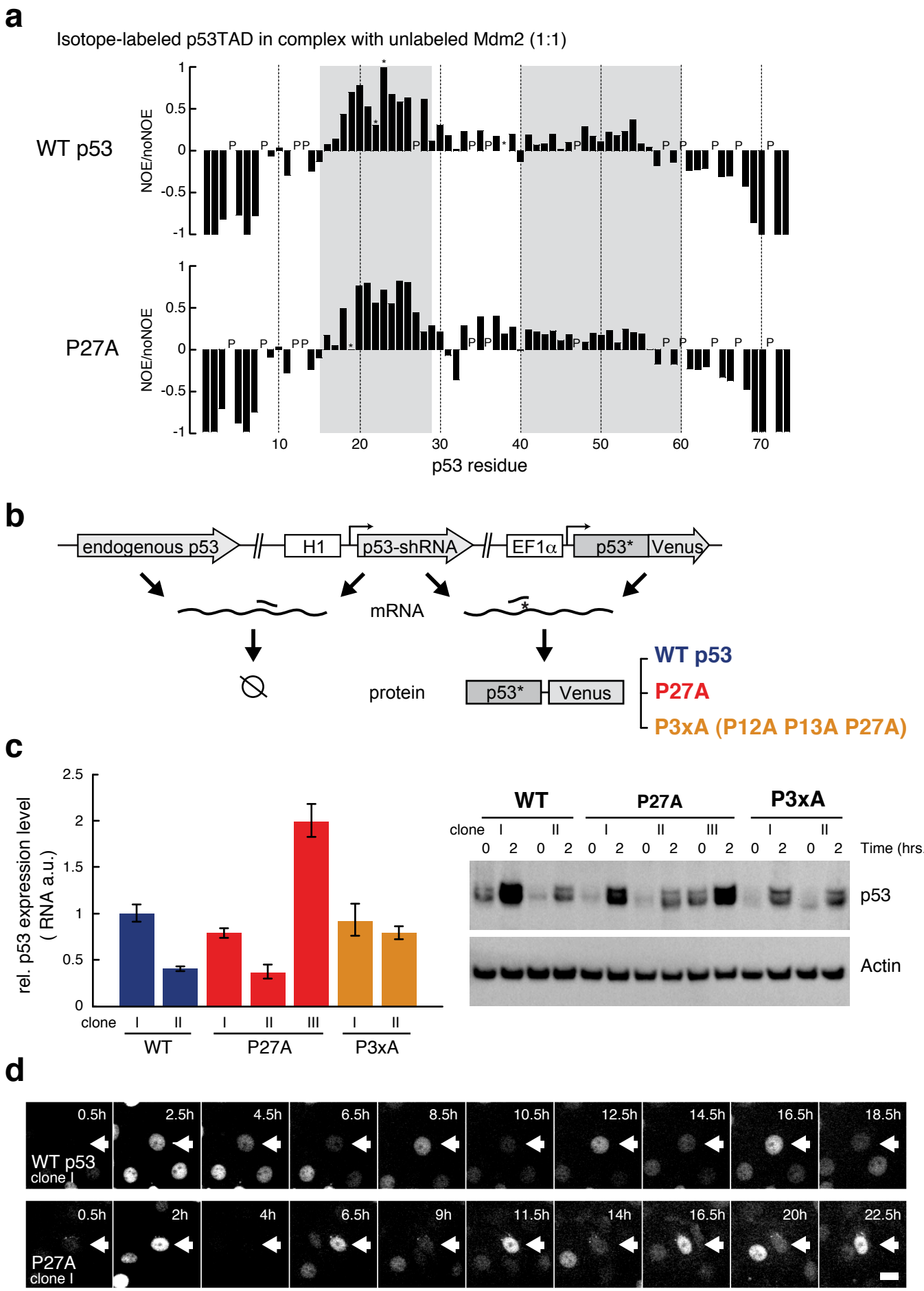
a
Isotope-labeled p53TAD in complex with unlabeled Mdm2 (1:1)
WT p53
P27A
NOE/noNOE
p53 residue
b
endogenous p53
H1
p53-shRNA
EF1α
p53*
Venus
mRNA
protein
WT p53
P27A
P3xA (P12A P13A P27A)
c
rel. p53 expression level (RNA a.u.)
clone
WT
P27A
P3xA
Time (hrs.)
p53
Actin
d
WT p53 clone I
P27A clone I

Supplementary Figure 4: Cell models to study WT and helical p53TAD mutants and their dynamics

a) Hetero-nuclear NHNOE data for WT and P27A mutant p53TAD in complex with Mdm2. Sites of p53TAD prolines are indicated. Asterisks denote residues with very weak peak intensities in the bound state. **b)** Schematic overview of procedures used for shRNA-mediated repression of endogenous p53 and expression of Venus-tagged versions of WT and mutant p53. **c)** Bar graphs show clonal variations in WT and mutant p53 mRNA expression levels in the different MCF7 cell clones as determined by RT-qPCR. Data are normalized to WT clone I, Actin serves as the internal standard. Error bars represent standard deviations. Western blot analysis of basal and DNA damaged-induced p53 levels for the different cell clones. (Uncropped Western blot images are shown in **Supplementary Figure 10**). **d)** Representative time series of live-cell fluorescence images showing oscillating protein levels of WT and P27A mutant p53. Arrows mark the same cell at each time point; the scale bar indicates 20 μm.

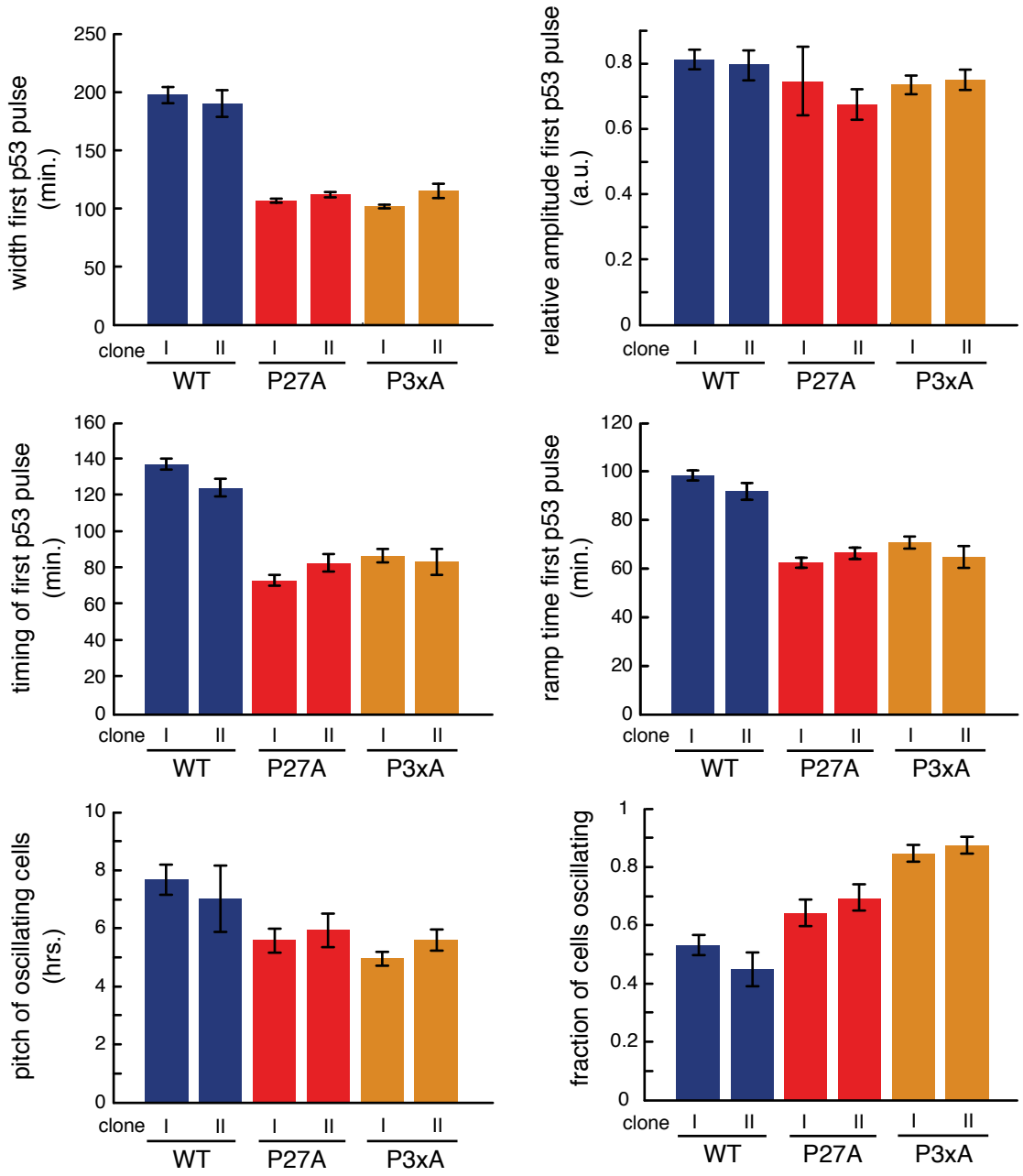
width first p53 pulse (min.)
250
200
150
100
50
0
clone I II I II I II
WT P27A P3xA
relative amplitude first p53 pulse (a.u.)
0.8
0.6
0.4
0.2
0
clone I II I II I II
WT P27A P3xA
timing of first p53 pulse (min.)
160
140
120
100
80
60
40
20
0
clone I II I II I II
WT P27A P3xA
ramp time first p53 pulse (min.)
120
100
80
60
40
20
0
clone I II I II I II
WT P27A P3xA
pitch of oscillating cells (hrs.)
10
8
6
4
2
0
clone I II I II I II
WT P27A P3xA
fraction of cells oscillating
1
0.8
0.6
0.4
0.2
0
clone I II I II I II
WT P27A P3xA

Supplementary Figure 5: Quantification of pulsed accumulation profiles of WT and mutant p53 cells

Dynamic features were quantified from single cell trajectories and are indicated on the corresponding y-axes of the bar graphs. Error bars represent standard error of the mean and standard error of the proportion, respectively. $n > 100$ cells per condition.

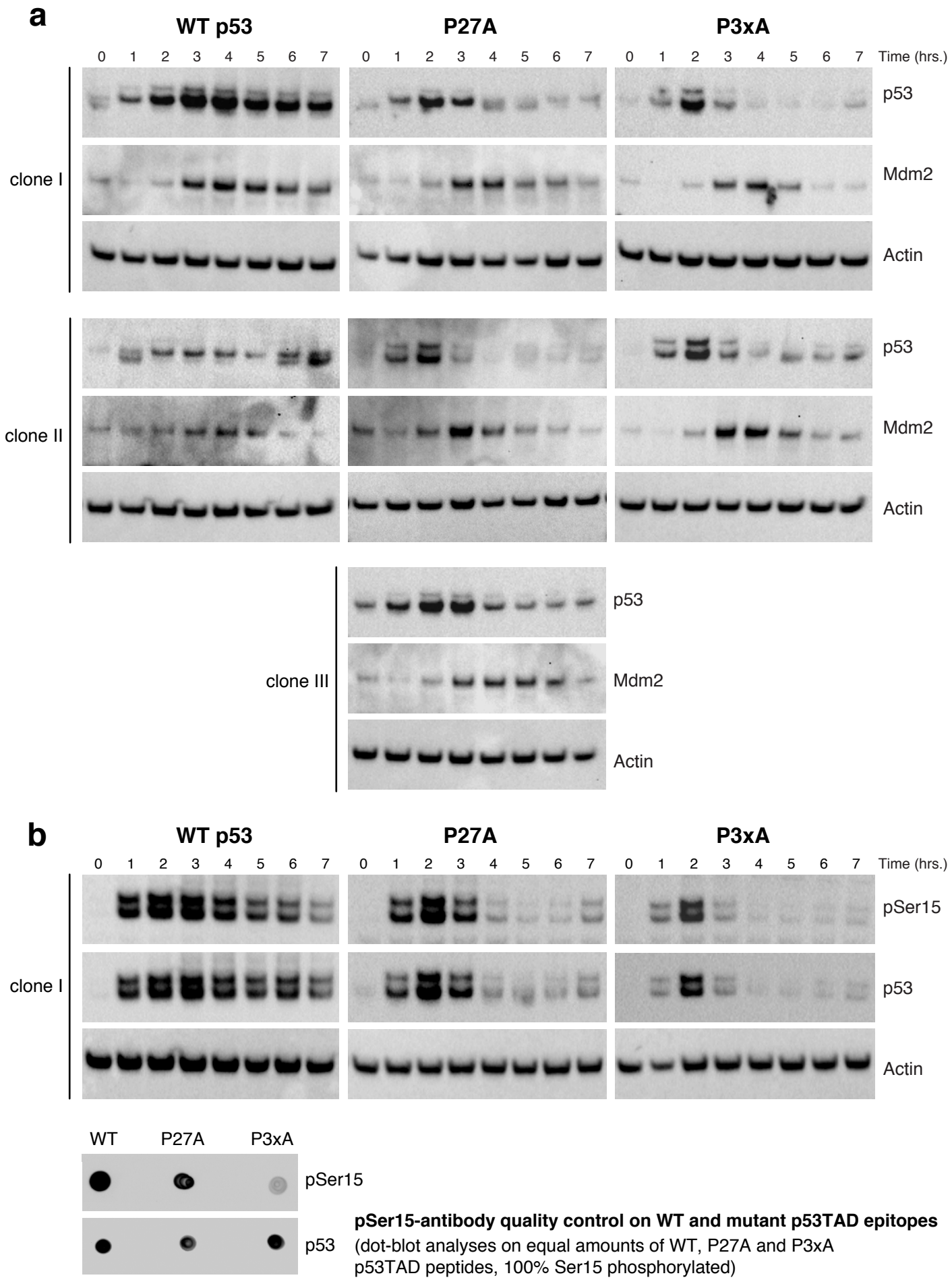

pSer15-antibody quality control on WT and mutant p53TAD epitopes
(dot-blot analyses on equal amounts of WT, P27A and P3xA p53TAD peptides, 100% Ser15 phosphorylated)

Supplementary Figure 6: Cellular dynamics and phosphorylation of WT and P27A, P3xA p53

a) Time-resolved Western blots of WT and mutant p53 accumulation profiles upon DSB induction and correlation with Mdm2 protein levels. **b)** Time resolved Western blots of total and Ser15-phophorylated p53. Actin serves as the loading control in all cases. Bottom panel: Dot-blot analysis of anti-pSer15 antibody detection efficiency of P27A and P3xA mutated p53TAD epitopes. (Uncropped Western blot images are shown in **Supplementary Figure 10**).

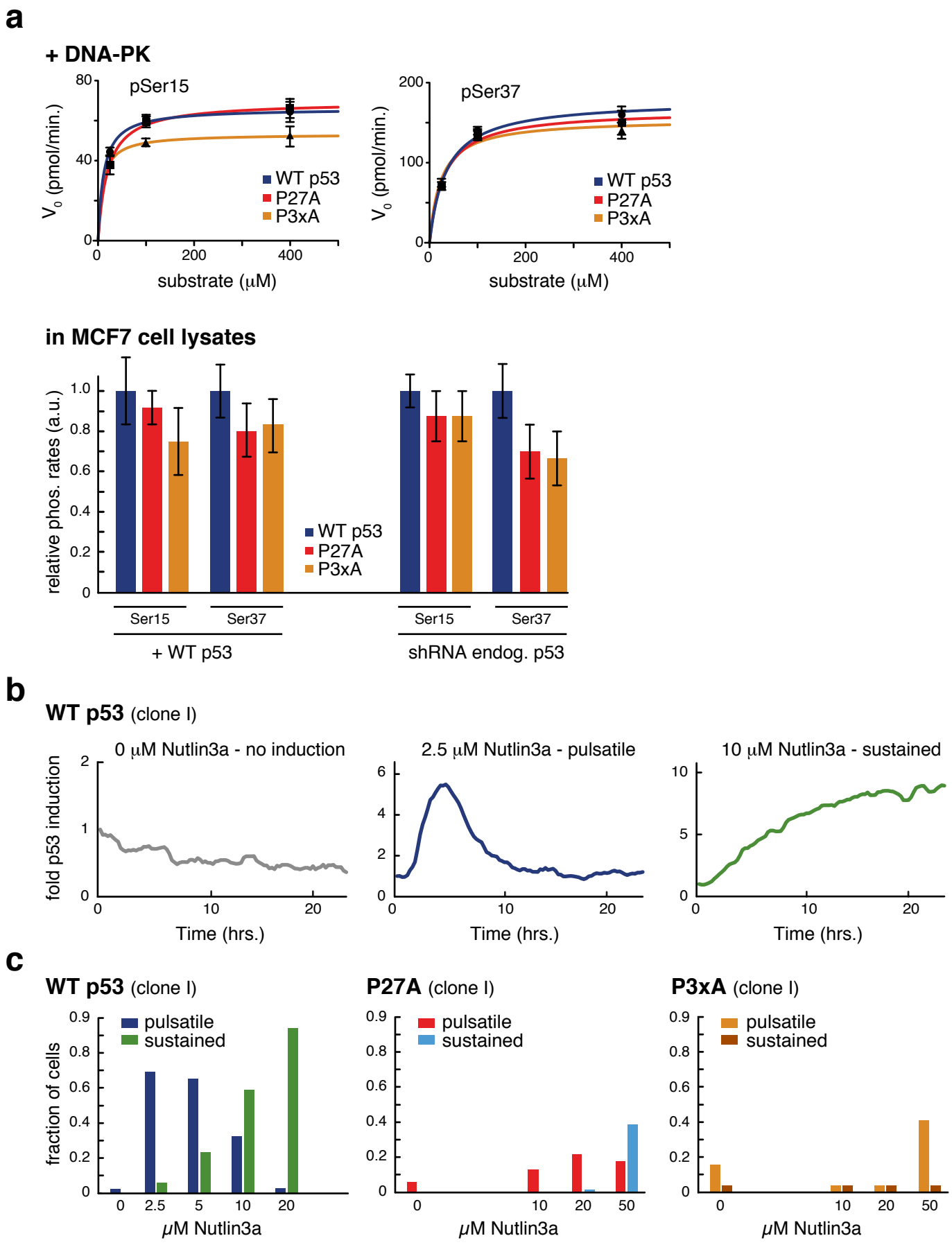
a
+ DNA-PK
pSer15
pSer37
V0 (pmol/min.)
substrate (μM)
WT p53
P27A
P3xA
in MCF7 cell lysates
relative phos. rates (a.u.)
Ser15
Ser37
+ WT p53
shRNA endog. p53
b
WT p53 (clone I)
0 μM Nutlin3a - no induction
2.5 μM Nutlin3a - pulsatile
10 μM Nutlin3a - sustained
fold p53 induction
Time (hrs.)
c
WT p53 (clone I)
P27A (clone I)
P3xA (clone I)
pulsatile
sustained
fraction of cells
μM Nutlin3a

Supplementary Figure 7: Phosphorylation and effects of Nutlin3a on WT and mutant p53

a) Time-resolved NMR measurements of initial Ser15 and Ser37 phosphorylation velocities of WT and mutant p53TAD with recombinant DNA-PK. Direct time-resolved NMR measurements of relative phosphorylation rates of WT and mutant p53TAD by endogenous kinases in MCF7 cell lysates in the absence (shRNA endog. p53, right part), or re-introduced presence of full-length, WT p53 (left part). Rates of WT p53TAD were normalized and mutant rates determined with respect to WT. All NMR experiments were carried out in duplicates. Error bars represent standard deviations. **b)** Exemplary single cell trajectories of WT p53 dynamics after treatment with different concentrations of Nutlin3a. **c)** Quantifications of cells displaying pulsatile versus sustained p53 accumulations at different concentrations of Nutlin3a in WT and mutant backgrounds. p53 accumulations were considered 'sustained' if levels stayed above 67% of peak levels for the duration of the experiment. $n > 60$ cells per condition.

a

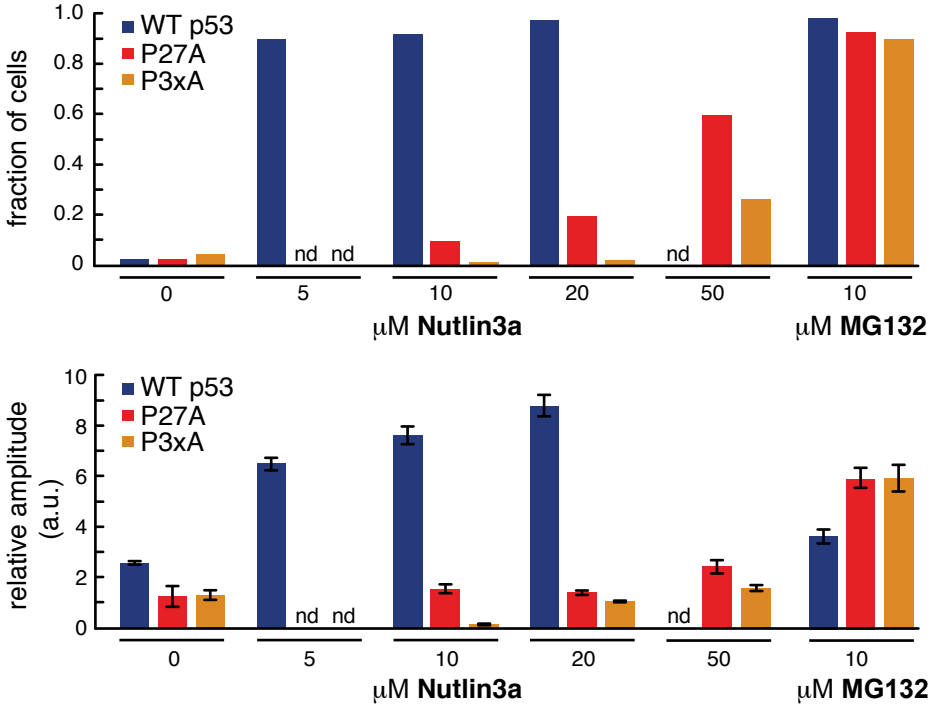
Effects of Nutlin3a versus MG132 (all clone I)
WT p53
P27A
P3xA
fraction of cells
1.0
0.8
0.6
0.4
0.2
0
nd nd
nd
0
5
10
20
50
10
μM Nutlin3a
μM MG132
relative amplitude (a.u.)
10
8
6
4
2
0

b

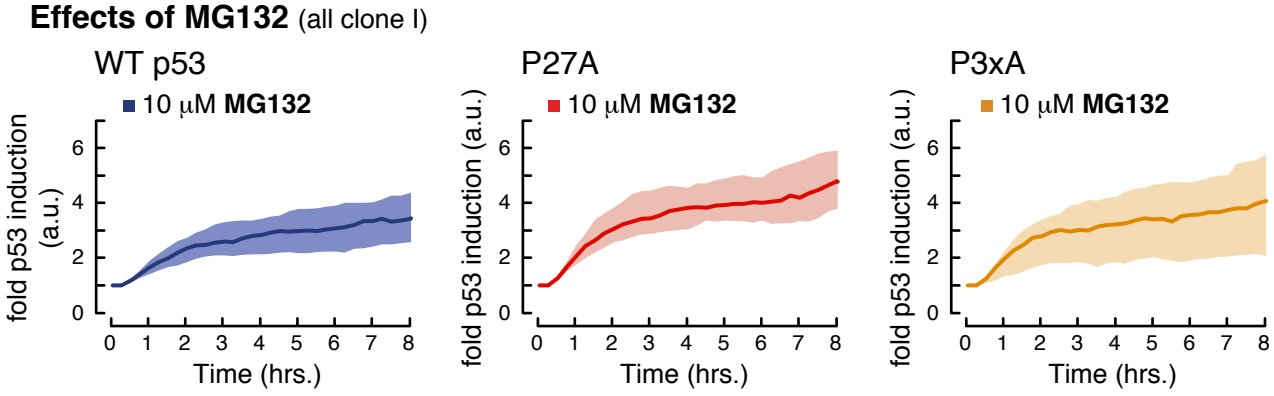
Effects of MG132 (all clone I)
WT p53
P27A
P3xA
10 μM MG132
fold p53 induction (a.u.)
Time (hrs.)
0 1 2 3 4 5 6 7 8

c

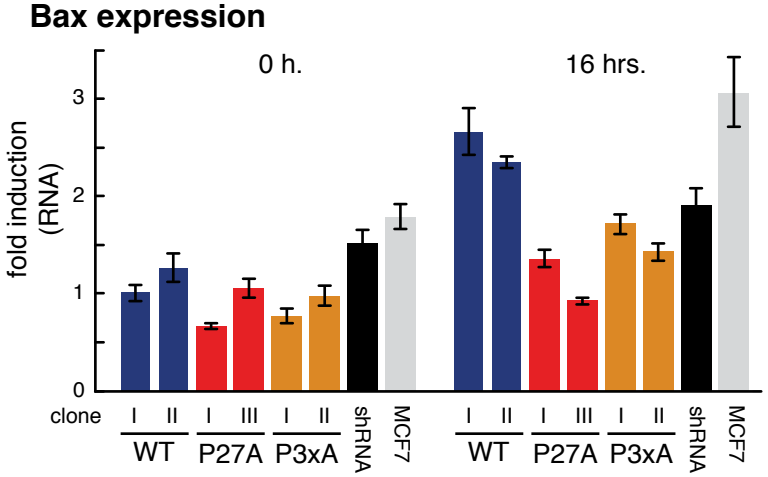
Bax expression
0 h.
16 hrs.
fold induction (RNA)
3
2
1
0
clone
I II I III I II shRNA MCF7
WT P27A P3xA

Supplementary Figure 8: Nutlin3a and MG132 effects, and p53 target gene expression

a) Comparative analysis of the fraction of cells with induced p53 expression and amplitudes of p53 accumulations upon Nutlin3a and MG132 treatment. n > 60 cells per condition. **b)** Time evolution of p53 accumulation in cells expressing WT and mutant p53 upon proteasome inhibition with MG132. Solid lines indicate the mean, shaded areas the standard deviations of accumulated responses. n > 60 cells per condition. **c)** Measured differences of Bax mRNA levels in cells carrying wt and mutant p53, before and 16 hours after DSB induction. Bax levels with background p53 after shRNA knockdown (black) and with endogenous p53 in non-manipulated MCF7 cells (grey). Error bars represent standard deviations of technical replicates. Data is representative for duplicate experiments.

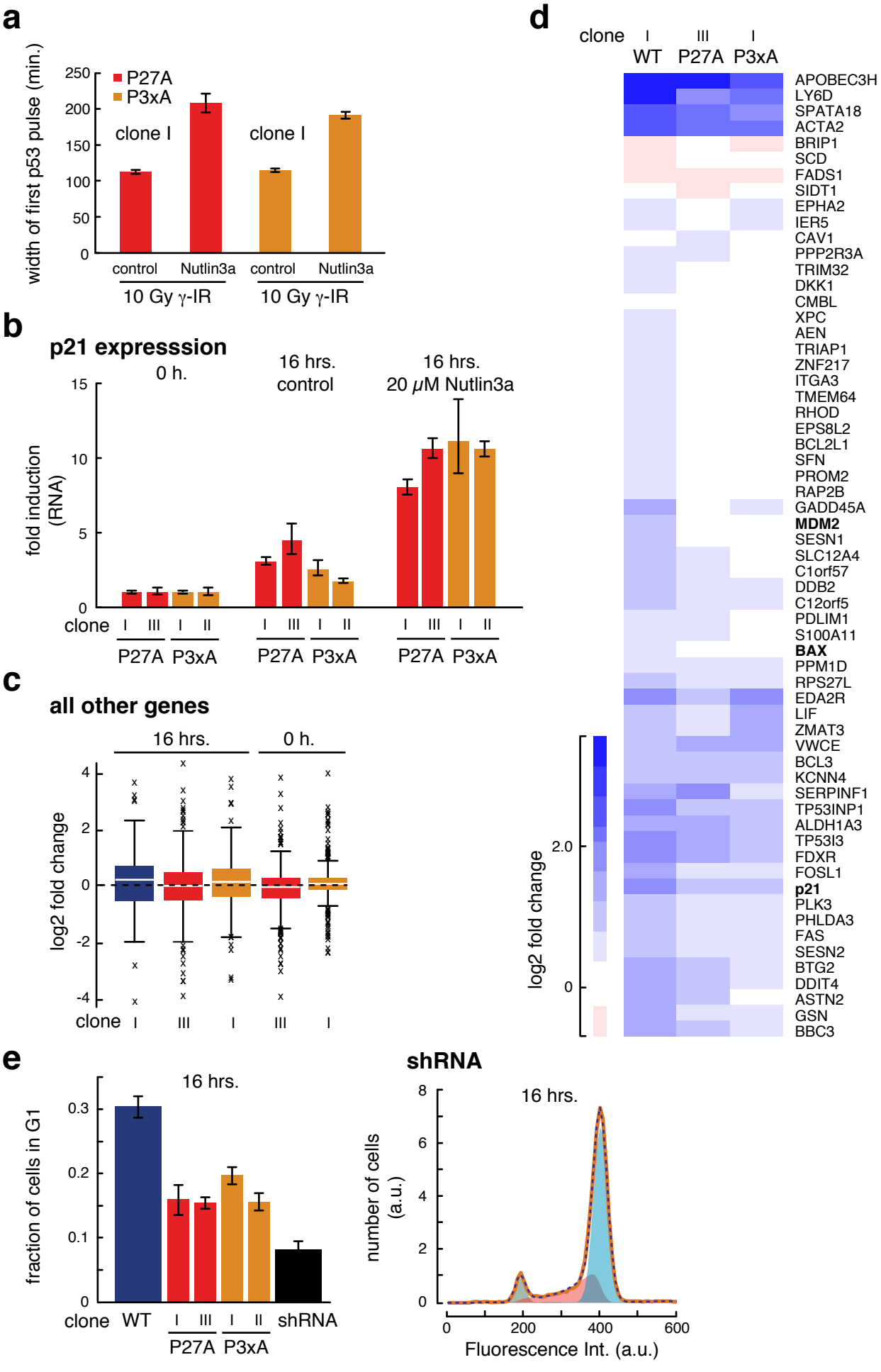
a
width of first p53 pulse (min.)
P27A
P3xA
clone I
clone I
control
Nutlin3a
control
Nutlin3a
10 Gy γ-IR
10 Gy γ-IR
b
p21 expresssion
0 h.
16 hrs. control
16 hrs. 20 μM Nutlin3a
fold induction (RNA)
clone
P27A P3xA
c
all other genes
16 hrs.
0 h.
log2 fold change
clone
d
clone
WT P27A P3xA
log2 fold change
APOBEC3H
LY6D
SPATA18
ACTA2
BRIP1
SCD
FADS1
SIDT1
EPHA2
IER5
CAV1
PPP2R3A
TRIM32
DKK1
CMBL
XPC
AEN
TRIAP1
ZNF217
ITGA3
TMEM64
RHOD
EPS8L2
BCL2L1
SFN
PROM2
RAP2B
GADD45A
MDM2
SESN1
SLC12A4
C1orf57
DDB2
C12orf5
PDLIM1
S100A11
BAX
PPM1D
RPS27L
EDA2R
LIF
ZMAT3
VWCE
BCL3
KCNN4
SERPINF1
TP53INP1
ALDH1A3
TP53I3
FDXR
FOSL1
p21
PLK3
PHLDA3
FAS
SESN2
BTG2
DDIT4
ASTN2
GSN
BBC3
e
16 hrs.
fraction of cells in G1
clone WT
P27A P3xA
shRNA
shRNA
16 hrs.
number of cells (a.u.)
Fluorescence Int. (a.u.)

Supplementary Figure 9: Altered target gene expression- and cell cycle-profiles of helical p53TAD mutants in response to DNA damage

a) Widths of p53 pulses post damage in P27A and P3xA mutant backgrounds in the presence or absence of 20 μM Nutlin3a (added 60 min. after irradiation). Error bars represent standard error of the mean. n > 60 cells per condition. **b)** Measured p21 mRNA levels in cells carrying mutant p53 16 hours post DSB induction in the presence, or absence of 20 μM Nutlin3a, compared to levels before damage. Actin serves as the internal standard for mRNA quantifications. Error bars represent standard error of the mean. n > 60 cells per condition. **c)** Distributions of log2-fold changes of differentially expressed non-p53 target genes before and after DSB induction. Data are normalized to expression levels of each gene in WT p53 cells before irradiation (0 h). White lines indicate the median of distributions, boxes include data between the 25^{th} and 75^{th} percentile. Whiskers extend to maximum values that are within 1.5 times the interquartile range; crosses represent outliers. Samples were sequenced on two lanes (rapid run mode); sequencing depth was 250 million reads. **d)** Heat map of fold-differences in p53 target gene inductions 16 hours post DSB in WT and mutant cells as determined by genome-wide RNAseq measurements. **e)** Summary of the fraction of G1 cells in WT, mutant and shRNA-depleted p53 cells. DNA contents measured by flow cytometry and cell stage distributions in shRNA-depleted p53 cells 16 hours post DSB. Actin serves as the internal standard for mRNA quantifications. Data is from triplicate experiments; error bars represent standard error of the mean.

Supplementary Figure 10

Borcherds *et al.*

uncropped Western blots **Supplementary Figure 4c**

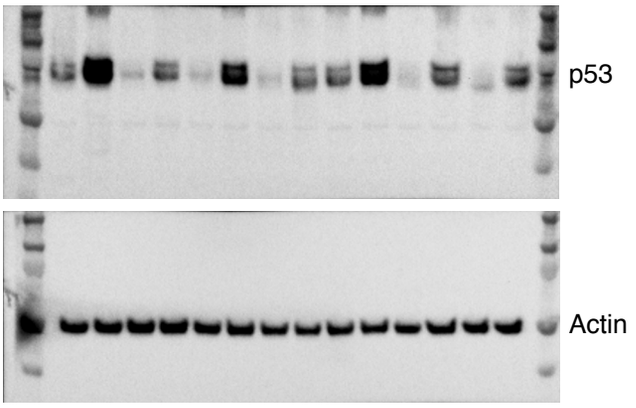

uncropped Western blots **Supplementary Figure 6a**

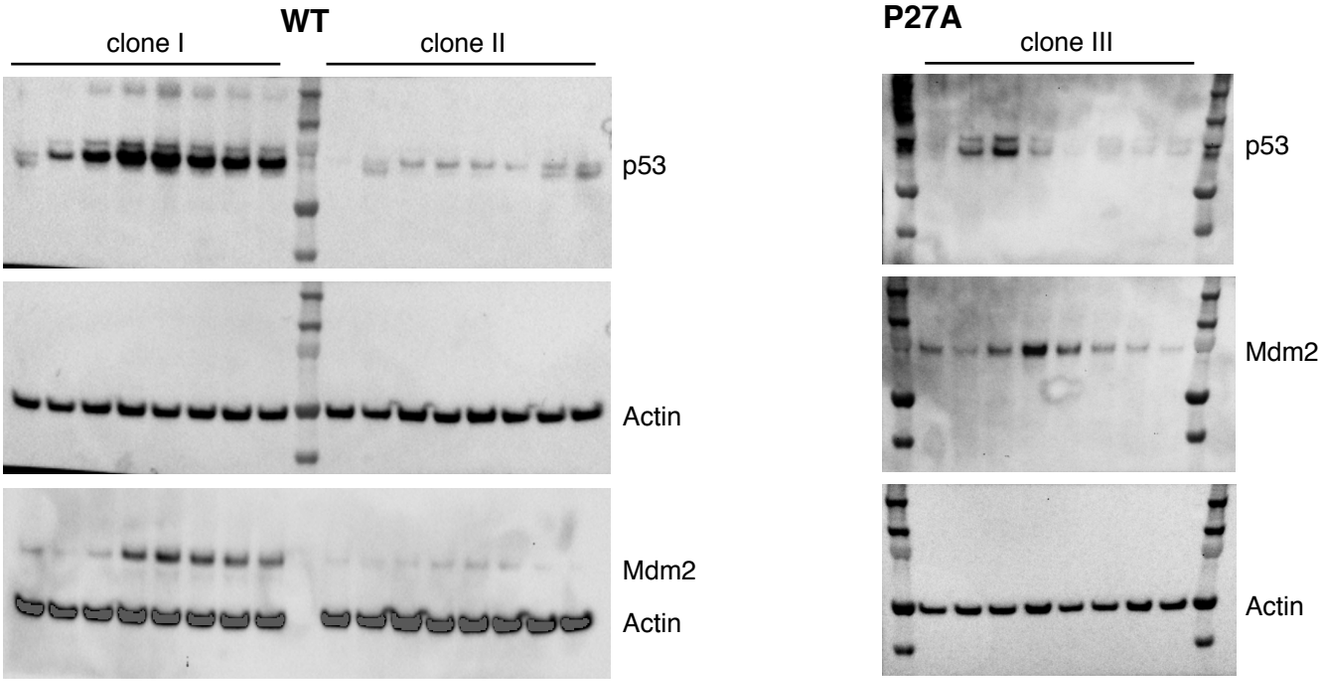

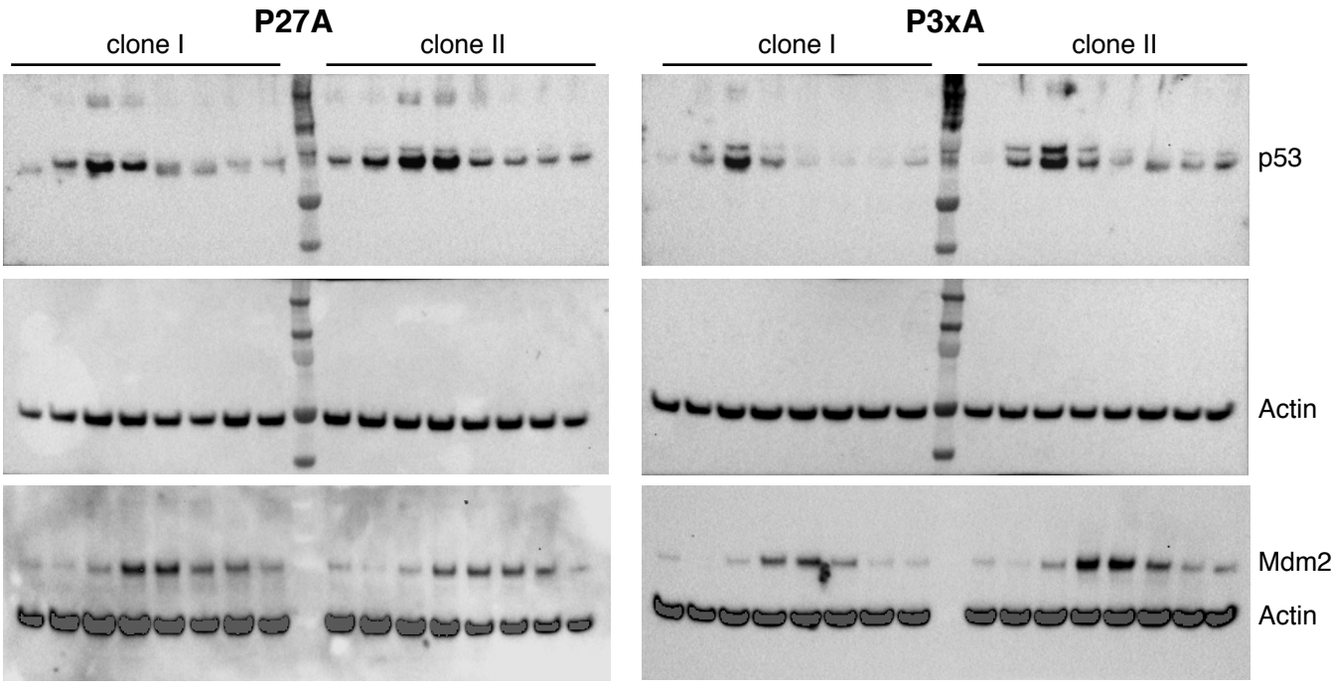

uncropped Western blots **Supplementary Figure 6b**